NANO · MICRO small
www.small-journal.com

3D Hydrazone-Functionalized Covalent Organic Frameworks as pH-Triggered Rotary Switches

Wenjuan Zhao, Chengyang Yu, Jie Zhao, Fengqian Chen, Xinyu Guan, Hui Li, Bin Tang, Guangtao Yu, Valentin Valtchev, Yushan Yan, Shilun Qiu, and Qianrong Fang**

The property expansion of 3D functionalized covalent organic frameworks (COFs) is important for developing their potential applications. Herein, the first case of 3D hydrazone-decorated COFs as pH-triggered molecular switches is reported, and their application in the stimuli-responsive drug delivery system is explored. These functionalized COFs with hydrazone groups on the channel walls are obtained via a multi-component bottom–up synthesis strategy. They exhibit a reversible *E*/*Z* isomerization at various pH values, confirmed by UV–vis absorption spectroscopy and proton conduction. Remarkably, after loading cytarabine (Ara-C) as a model drug molecule, these pH-responsive COFs show an excellent and intelligent sustained-release effect with an almost fourfold increase in the Ara-C release at pH = 4.8 than at pH = 7.4, which will effectively improve drug-targeting. Thus, these results open a way toward designing 3D stimuli-responsive functionalized COF materials and promote their potential application as drug carriers in the field of disease treatment.

1. Introduction

Covalent organic frameworks (COFs) are a new class of crystalline porous polymers that allow crystallographically precise integration of building blocks into periodic structures.[1] The potential applications of COFs are in various fields, including gas adsorption and separation,[2] organic electronics,[3] heterogeneous catalysis,[4] and others.[5] At present, most of the discovered COFs are still 2D frameworks with eclipsed stacking structures because of their simpler synthesis and easier functionalization. Compared with 2D analogues, 3D functionalized COFs have recently attracted more and more attention due to their unique pore structures and higher specific surface areas.[6] For example, we have acquired a series of 3D functionalized COFs,[7] for example, 3D tetrathiafulvalene-based COFs for tunable electrical conductivity, 3D carboxy-functionalized COF for selective ion adsorption, and 3D Salphen-based COFs as catalytic antioxidants. Despite the aforementioned efforts in the in-situ synthesis and post-synthesis modifications, the functionalization of 3D COFs still remains largely undeveloped up to now, especially 3D architectures with stimuli-responsive functions,[8] due to the lacking of building units, the difficulty of directional synthesis, and the sophisticated procedure for introducing functional groups into the framework.

It is well-known that hydrazone and its derivatives are significant synthons for numerous transformations, and their C=N groups can undergo efficiently reversible structures between

W. Zhao, C. Yu, F. Chen, X. Guan, H. Li, S. Qiu, Q. Fang
State Key Laboratory of Inorganic Synthesis and Preparative Chemistry
Jilin University
Changchun 130012, P. R. China
E-mail: qrfang@jlu.edu.cn

J. Zhao
SINOPEC Research Institute of Petroleum Processing
Beijing 100083, P. R. China

B. Tang
Institute for Frontier Materials
Deakin University
Geelong, Victoria 3216, Australia
E-mail: bin.tang@deakin.edu.au

G. Yu
College of Chemistry and Materials Science
Fujian Normal University
Fuzhou 350007, P. R. China

V. Valtchev
Qingdao Institute of Bioenergy and Bioprocess Technology
Chinese Academy of Sciences
189 Songling Road, Laoshan District, Qingdao, Shandong 266101, P. R. China

V. Valtchev
Normandie Univ
ENSICAEN
UNICAEN
CNRS
Laboratoire Catalyse et Spectrochimie
6 Marechal Juin, Caen 14050, France

Y. Yan
Department of Chemical and Biomolecular Engineering
Center for Catalytic Science and Technology
University of Delaware
Newark, DE 19716, USA

The ORCID identification number(s) for the author(s) of this article can be found under https://doi.org/10.1002/smll.202102630.

DOI: 10.1002/smll.202102630

E and *Z* configurations in the presence of acid or base.[9] Consequently, pH-triggered hydrazone-based switches are widely incorporated into various materials,[10,11] including supramolecular systems, liquid crystals, polymer gels, and some 2D COFs to achieve such unique properties. However, although the combination of building blocks with hydrazone as side chains and the interconnected channels of 3D structures will be greatly beneficial for the development of stimuli-responsive materials, no hydrazone has been integrated into 3D COF materials so far because of the difficulties of crystallization and structural determination.

Herein, we report the synthesis of 3D hydrazone-equipped COFs and study their application as pH-triggered rotary switches in the stimuli-controlled release of the drug molecule. Different from previous reports, the hydrazone groups, in this case, were decorated on the channel walls of COFs using a multi-component bottom–up synthesis strategy. The obtained structures showed well-behaved invertibility of *E*/*Z* isomerization at different pH values, which was confirmed by proton conduction and UV–vis absorption analysis. More importantly, after loading drug molecule (cytarabine, Ara-C), these stimuli-responsive COFs demonstrated exceptional release effects for Ara-C with an almost fourfold amplification at pH = 4.8 than at pH = 7.4. This is the first example of 3D hydrazone-functionalized COFs and their application for pH-responsive drug delivery to the best of our knowledge.

2. Results and Discussion

2.1. Synthesis and Characterization

Our strategy for constructing 3D stimuli-responsive COFs is based on a hydrazone derivative with *E*/*Z* interconversion, (*E*)-ethyl-2-(2-(4,4″-diaminobiphenyl) hydrazono)-2-(pyridin-2-yl) acetate (HZ (*E*), **Scheme 1**a). To maximize the functionalization of materials while maintaining their crystallinity and porosity, we have employed a multi-component condensation system to synthesize a series of 3D COFs. As shown in Scheme 1b, 4,4″-diaminobiphenyl (DABP) and HZ (*E*) were chosen as linear linkers, while 1,3,5,7-tetrakis(4-formylphenyl) adamantane (TFPA) was designed as an ideal tetrahedral building unit. The condensation of TFPA with HZ (*E*) and DABP produced 3D COFs with different amounts of HZ (*E*), JUC-556-$[HZ]_X$ (*E*), where *X* is the proportion of HZ (*E*) (X = [HZ (*E*)]/([DABP] + [HZ (*E*)])); *X* = 0.25, 0.50, 0.75, or 1.00; Scheme 1c). Similar to HZ (*E*) building unit, JUC-556-$[HZ]_X$ (*E*) also displayed the excellent acid/base controlled *E*/*Z* isomerization (Scheme 1d). Composed from linear and tetrahedral building blocks and subjected to the large steric effect of HZ (*E*) groups, these COFs are expected to exhibit a twofold interpenetrated diamondoid (dia) network (Scheme 1e).[12]

Typically, JUC-556-$[HZ]_X$ (*E*) were synthesized by suspending DABP and/or HZ (*E*) with TFPA in the mixed solvent of dioxane and mesitylene in the presence of acetic acid followed by heating at 120 °C for 3 days. These condensation reactions exhibited similar isolated yields (≈80%), indicating that the reactivities of DABP and HZ (*E*) were similar. Similar to previous reports, elemental analysis revealed that the ratios of HZ (*E*) to DABP integrated into JUC-556-$[HZ]_X$ (*E*) were identical to those employed for their reactions (Section S1, Supporting Information).[13] The structural characterization of JUC-556-$[HZ]_X$ (*E*) was executed combining complementary methods. Scanning electron microscopy indicated that JUC-556-$[HZ]_X$ (*E*) showed rod-shaped crystals (Figures S1–S4, Supporting Information). In Fourier transform infrared spectra of JUC-556-$[HZ]_X$ (*E*), the peaks assigned to C=N stretching vibration appeared at about 1615 cm^{-1}, demonstrating the formation of imine linkage (Figures S5–S8, Supporting Information). The solid-state ^{13}C cross-polarization magic-angle-spinning (CP/MAS) NMR spectra further confirmed the presence of imine linkage in the light of the distinguishing C=N signals at about 152 ppm for JUC-556-$[HZ]_X$ (*E*) (Figures S9–S12, Supporting Information). According to the thermogravimetric analysis, JUC-556-$[HZ]_X$ (*E*) began to lose weight at 250 °C due to the decomposition of the HZ (*E*) monomer while the overall skeleton was stable up to about 500 °C in the nitrogen atmosphere (Figures S13–S17, Supporting Information). Furthermore, the crystalline structures of JUC-556-$[HZ]_X$ (*E*) could be maintained in a variety of organic solvents and aqueous solutions with a series of pH values, especially in triethylamine, hydrochloric acid, and trifluoroacetic acid (TFA), verifying their remarkable stability (Figures S18–S21, Supporting Information).

The crystalline structures of JUC-556-$[HZ]_X$ (*E*) were revealed by powder X-ray diffraction (PXRD) analysis (**Figure 1**). Herein we took JUC-556-$[HZ]_{0.25}$ (*E*) as an example to analyze their structures (Figure 1a). The unit cell parameters of JUC-556-$[HZ]_{0.25}$ (*E*) were resolved by the PXRD pattern in conjunction with structural simulation. After a geometrical energy minimization by using the Materials Studio software package[14] based on a twofold interpenetrated dia net and disordered HZ (*E*), the unit cell parameters of JUC-556-$[HZ]_{0.25}$ (*E*) were obtained ($a = b$ = 28.2591 Å, c = 34.7253 Å, and $\alpha = \beta = \gamma = 90°$). The simulated PXRD pattern was in good agreement with the experimental one (Figure 1a). Furthermore, the full profile pattern matching (Pawley) refinement was performed from the experimental PXRD pattern. The strong PXRD peaks at 4.03°, 5.11°, 6.25°, 8.27°, 9.20°, 11.10°, 12.18°, 16.42°, and 18.98° 2θ can be assigned to the (101), (110), (200), (103), (221), (114), (303), (414), and (514) Bragg peaks of a tetragonal space group $P4_2/n$ (No. 86). The refinement results revealed that unit cell parameters were nearly equivalent to the predicted ones with excellent agreement factors ($a = b$ = 28.3520 Å, c = 34.8160 Å, $\alpha = \beta = \gamma = 90°$, ωR_p = 5.77%, and R_p = 4.29%). In addition, we also examined alternative structures, such as non-interpenetrated dia network. However, there were significant differences between the simulated and experimental PXRDs (Figures S22–S24, Supporting Information). As the HZ (*E*) content increases, the crystallinity of JUC-556-$[HZ]_X$ (*E*) decreases slightly due to disordered HZ (*E*) units on the channel walls; however, these materials also exhibit similar diffraction patterns, indicating that they have the same structures (Figure 1b–d). Based on the above results, it is proposed that JUC-556-$[HZ]_X$ (*E*) have the expected architectures with twofold interpenetrated dia nets, and microporous cavities with a diameter of about 1.70 nm (Scheme 1f).

The porosity and specific surface areas of JUC-556-$[HZ]_X$ (*E*) were analyzed by nitrogen gas adsorption measurements at 77 K (**Figure 2**). A sharp increase in gas uptake at low pressure

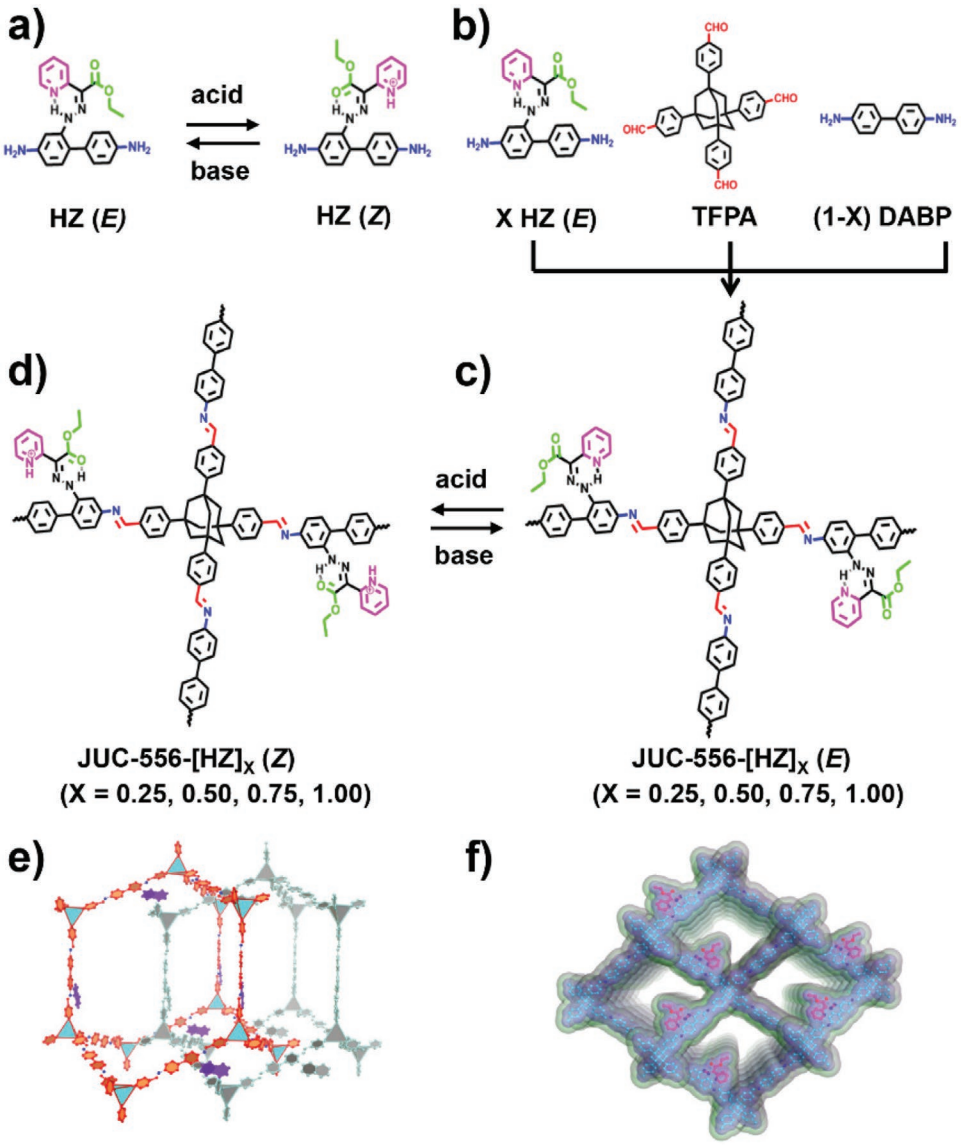

Scheme 1. Schematic representation of the strategy for preparing JUC-556-[HZ]$_X$ with *E*/*Z* isomerization. a) Acid/base controlled *E*/*Z* isomerization of free HZ molecule. b) Molecular structures of TFPA as a tetrahedral building unit as well as HZ (*E*) and DABP as linear linkers. c) JUC-556-[HZ]$_X$ constructed by the condensation reaction of TFPA with HZ (*E*) and DABP ($X = 0.25$, 0.5, 0.75, and 1.00). d) Acid/base controlled *E*/*Z* isomerization in JUC-556-[HZ]$_X$. e) Twofold interpenetrated dia network in JUC-556-[HZ]$_X$ (*E*). f) Structural representation of JUC-556-[HZ]$_X$ (*E*).

(below 0.1 P/P_0) demonstrated the microporous nature of JUC-556-[HZ]$_X$ (*E*). An inclination of the isotherm and slight desorption hysteresis were observed, implying the presence of textural mesopores caused by the agglomeration of COF crystals.[7d] Their surface areas exhibited a decreasing tendency with the increase of HZ (*E*) content. The Brunauer–Emmett–Teller (BET) surface areas were 634 $m^2\ g^{-1}$ for JUC-556-[HZ]$_{0.25}$ (*E*), 527 $m^2\ g^{-1}$ for JUC-556-[HZ]$_{0.50}$ (*E*), 467 $m^2\ g^{-1}$ for JUC-556-[HZ]$_{0.75}$ (*E*), and 430 $m^2\ g^{-1}$ for JUC-556-[HZ]$_{1.00}$ (*E*), respectively (Figures S25–S28, Supporting Information). Based on nonlocal density functional theory, JUC-556-[HZ]$_X$ (*E*) showed similar microporous diameters of 1.62–1.80 nm (Figures S29–S32, Supporting Information), which were in good agreement with the pore sizes predicted from their crystal structures (1.70 nm).

2.2. pH-Triggered *E*/*Z* Isomerization

Inspired by the abundant presence of HZ dangling groups, we studied the pH-triggered rotary switching effect of JUC-556-[HZ]$_X$ under different pH conditions (Figures S33–S62, Supporting Information). The acid/base induced *E*/*Z* isomerization of dissociative HZ units was inspected by UV–vis absorption spectroscopy and ^{1}H NMR, and the results clearly showed that the pH-triggered switching process was reversible (Figures S33–S44, Supporting Information). Similar to free HZ, JUC-556-[HZ]$_X$ also exhibited good pH-responsive switching behaviors. The color of the as-synthesized JUC-556-[HZ]$_X$ (*E*) evolved gradually from yellow to red upon acid treatment, and then went back to yellow when the base was added (**Figure 3**e; Figure S45, Supporting Information). Furthermore,

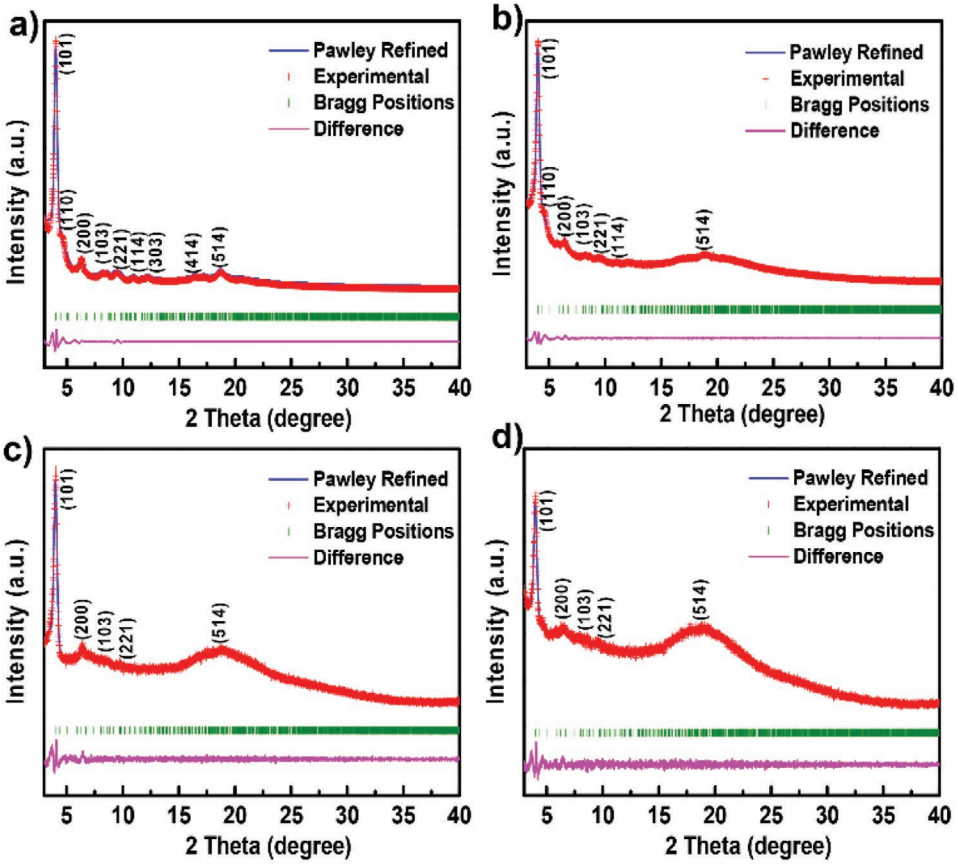

Figure 1. PXRD patterns of a) JUC-556-$[HZ]_{0.25}$ (*E*), b) JUC-556-$[HZ]_{0.50}$ (*E*), c) JUC-556-$[HZ]_{0.75}$ (*E*), and d) JUC-556-$[HZ]_{1.00}$ (*E*).

the evolution of UV–vis absorption spectra verified the *E*/*Z* configurational changes. JUC-556-$[HZ]_{0.50}$ (*E*) was selected as an example to illustrate the acid–base isomerization. When JUC-556-$[HZ]_{0.50}$ (*E*) was titrated with TFA (Figure 3a; Figure S46, Supporting Information), the intensity of the absorption band at 283 nm decreased whereas that at 249 nm increased as the amount of the added acid increased. The spectral conversion clearly indicated that the HZ groups of the JUC-556-$[HZ]_{0.50}$ (*E*) underwent the configurational changes from *E* to *Z*. Upon the addition of triethylamine (Et_3N) to the sample of JUC-556-$[HZ]_{0.50}$ (*Z*) (Figure 3b; Figure S47, Supporting Information), the absorption band of 283 nm restored, accompanying with the declining of the absorption band at 249 nm. JUC-556-$[HZ]_{0.50}$ (*E*) also showed good pH-triggered switching processes upon the addition of TFA/Et_3N with low concentrations and remarkable reversibility (Figure 3c,d). Notably, one isosbestic point at around 263 nm was observed, which clearly indicated the interconversion of two species of JUC-556-$[HZ]_X$ upon the variation of pH values. In addition, the transformation of colors and UV–vis absorption spectra of JUC-556-$[HZ]_X$ were slightly different from those of free HZ, which could be caused by steric hindrance and confinement effects of COF channels as well as potential inductive effects of atoms around HZ units.[15] Furthermore, the spectral conversion of JUC-556-$[HZ]_{0.50}$ (*E*) occurred with other acids, such as HCl (Figure 3f; Figure S48, Supporting Information). As for other JUC-556-$[HZ]_X$ (*E*), similar acid/base dependent changes of UV–vis absorption spectra were observed, and their *E*/*Z* configurations were also reversible under acidic/basic conditions (Figures S49–S62, Supporting Information).

Furthermore, the *E*/*Z* isomerization of JUC-556-$[HZ]_X$ was demonstrated by proton conduction at room temperature (**Figure 4**; Figures S63–S66, Supporting Information). As HZ (*E*) has rich nitrogen atoms, it can combine with HCl to form hydrogen bonds,[16] and therefore the as-synthesized JUC-556-$[HZ]_X$ (*E*) possessed the ability to accept protons. Typically, JUC-556-$[HZ]_X$ (*E*) were compressed into cylindrical pellets with a diameter of 6.0 mm and a thickness of 1.0 mm. The proton conductivities of the original JUC-556-$[HZ]_X$ (*E*) were 2.73×10^{-6} S m^{-1} for JUC-556-$[HZ]_{0.25}$ (*E*), 3.70×10^{-7} S m^{-1} for JUC-556-$[HZ]_{0.50}$ (*E*), 1.32×10^{-6} S m^{-1} for JUC-556-$[HZ]_{0.75}$ (*E*), and 3.91×10^{-7} S m^{-1} for JUC-556-$[HZ]_{1.00}$ (*E*), respectively. Remarkably, upon protonation with HCl vapor, the proton conductivities of activated JUC-556-$[HZ]_X$ (*Z*) increased up to 4.41×10^{-4} S m^{-1} for JUC-556-$[HZ]_{0.25}$ (*Z*), 7.04×10^{-4} S m^{-1} for JUC-556-$[HZ]_{0.50}$ (*Z*), 2.17×10^{-4} S m^{-1} for JUC-556-$[HZ]_{0.75}$ (*Z*), and 3.30×10^{-4} S m^{-1} for JUC-556-$[HZ]_{1.00}$ (*Z*), which are 162-fold, 1903-fold, 164-fold, and 844-fold improvement than those of the original ones, respectively. In addition, the proton conductivity dropped when the JUC-556-$[HZ]_X$ (*Z*) were treated with Et_3N vapor, indicating that the pH switching process was reversible. The proton conductivity could be maintained after three cycles (Figure S67, Supporting Information).

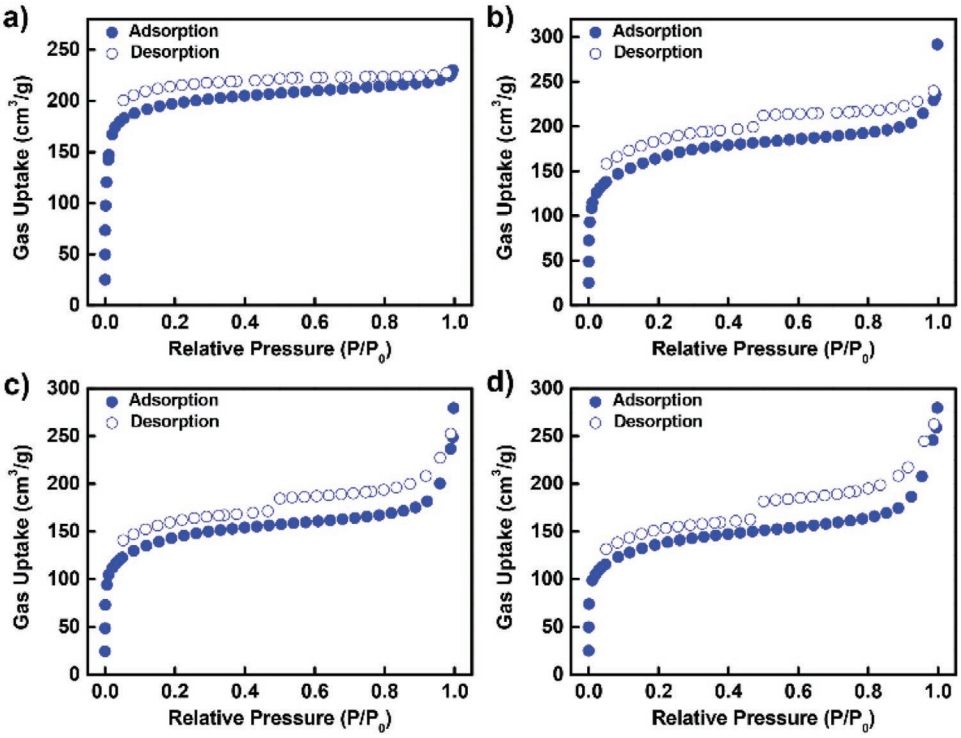

Figure 2. N_2 adsorption-desorption isotherms for a) JUC-556-$[HZ]_{0.25}$ (*E*), b) JUC-556-$[HZ]_{0.50}$ (*E*), c) JUC-556-$[HZ]_{0.75}$ (*E*), and d) JUC-556-$[HZ]_{1.00}$ (*E*) at 77 K.

2.3. pH-Responsive Drug Release

Given the high porosity and stability of JUC-556-$[HZ]_X$ (*E*) as well as favorable pH-responsive HZ units, we explored their potential application in the stimuli-responsive drug delivery system. Ara-C with a molecular size of about 0.9 nm was chosen as a model molecule because it is a traditional drug for cancer therapy, especially for pancreatic cancer, acute myelogenous leukemia, and chronic lymphoma.[17] Typically, the JUC-556-$[HZ]_X$ (*E*) were immersed in Ara-C aqueous solution for 9 h under stirring at 200 rpm, and Ara-C-loaded JUC-556-$[HZ]_X$ (*E*) were confirmed by UV–vis absorption spectra (Figure S68, Supporting Information). Then, the mixtures were filtered and washed. The resultant PXRD peaks were coincided with those of starting materials, confirming the structural integrity after loading Ara-C (Figures S69–S72, Supporting Information). As can be seen from nitrogen adsorption isotherms, the relevant porosity data after loading Ara-C showed significantly reduced BET surface areas (Figures S73–S76, Supporting Information). Each Ara-C-loaded JUC-556-$[HZ]_X$ (*E*) was transferred to two ampoules containing 5.0 mL releasing buffer solution separately, and the maximum UV–vis absorption intensity at 272 nm was chosen to indicate the drug concentration during the drug-releasing process. It is known that the cancer tissues generally exist in acidic extracellular environments with pH = 4 to 6. Therefore, we chose acetic acid buffer with pH = 4.8 as simulated cancer fluid to release the drug. The pH value in the normal physiological environment is almost neutral, and so a phosphate buffer (pH = 7.4) was used to simulate normal body fluid.[18] All JUC-556-$[HZ]_X$ showed smart drug sustained-release effects in two buffer solutions (**Figure 5**b; Figures S77–S79, Supporting Information). Among them, JUC-556-$[HZ]_{0.50}$ displayed the best performance in the release of drug, and the release rate reached 74.56% in the pH = 4.8 buffer within 72 h (*Z* isomerization), but only 18.59% in the pH = 7.4 buffer (*E* isomerization, Figure 5b). The release rate of drug molecule under acidic condition was nearly fourfold higher than that under neutral condition, greatly improving the drug targeting delivery and reducing its side effects. Furthermore, JUC-556-$[HZ]_{0.50}$ with *E* or *Z* isomerization exhibited reproducible identical effect for the capture and release of Ara-C even after five cycles (Figure 5c).

As for the drug release mechanism, it is suggested that the HZ unit as a pH-responsive rotary switch in JUC-556-$[HZ]_X$ plays a key role, which can form a variety of hydrogen bonds with drug molecules.[19] When the solution is neutral or basic, the hydrogen bonds between Ara-C and HZ (*E*) units promote the loading of Ara-C onto JUC-556-$[HZ]_X$ (*E*). Meanwhile, the channels of JUC-556-$[HZ]_X$ (*E*) provide the platforms for encapsulating Ara-C. On the contrary, when the surrounding is acidic, JUC-556-$[HZ]_X$ (*E*) transforms to *Z*-type configuration through the protonation of pyridine subunits, and simultaneously Ara-C was also protonated. The repulsive effect between JUC-556-$[HZ]_X$ (*Z*) and Ara-C can drive the high-efficiency release of Ara-C at the acidic condition (Figure 5a).

To further verify the mechanism of JUC-556-$[HZ]_X$ for the drug adsorption and release, we generated electrostatic potential (ESP) mapped van der Waals surfaces using Multiwfn software (Figure S80, Supporting Information)[20] and performed DFT calculations using Gaussian09 program packages

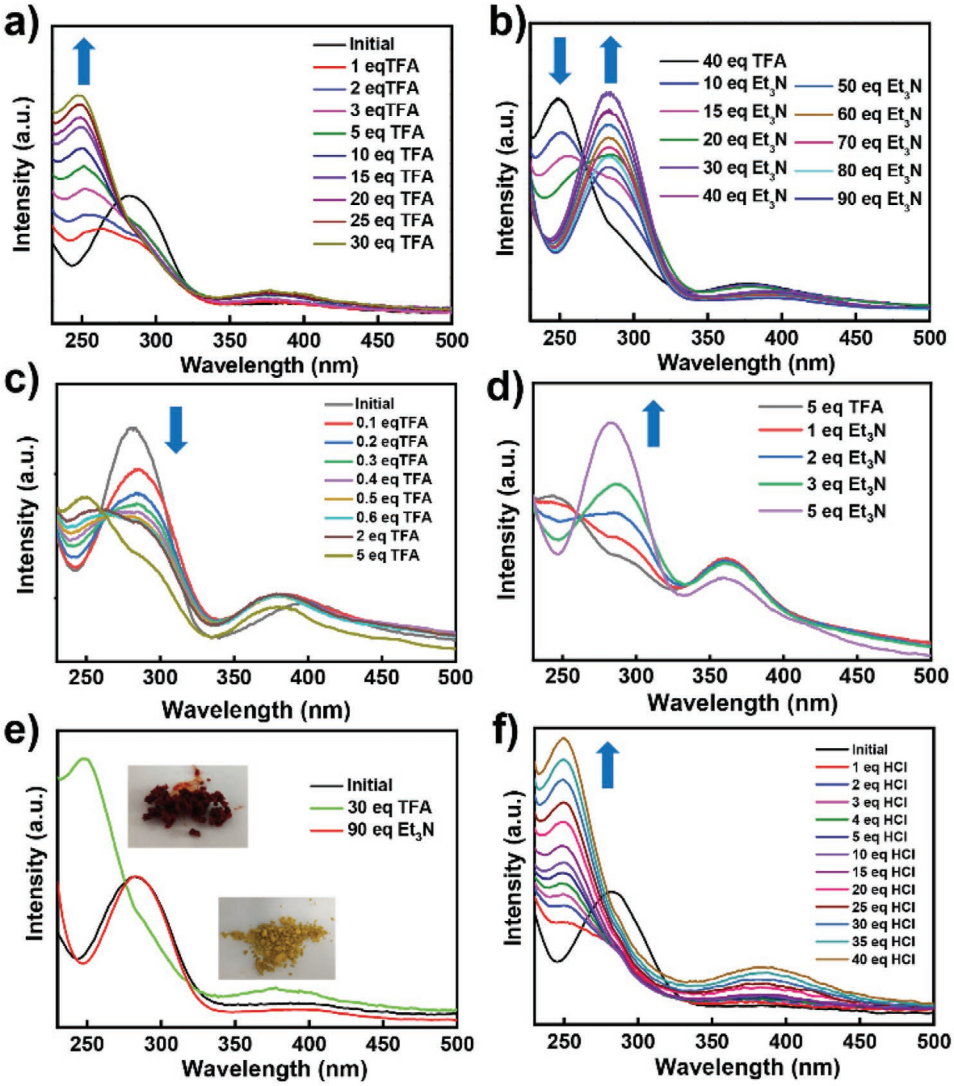

Figure 3. a) Absorption spectra of JUC-556-$[HZ]_{0.50}$ (*E*) upon protonation in TFA solution with increasing concentrations. b) Absorption spectra of JUC-556-$[HZ]_{0.50}$ (*Z*) upon deprotonation in Et_3N solution with increasing concentrations. c) Absorption spectra of JUC-556-$[HZ]_{0.50}$ (*E*) upon protonation in TFA solution under low concentrations. d) Absorption spectra of JUC-556-$[HZ]_{0.50}$ (*Z*) upon deprotonation in Et_3N solution under low concentrations. e) Reversible change of JUC-556-$[HZ]_{0.50}$ (*E*) in the acid/base solution. Inset: the color change of JUC-556-$[HZ]_{0.50}$ (*E*). f) Absorption spectra of JUC-556-$[HZ]_{0.50}$ (*E*) upon protonation in HCl solution with increasing concentrations.

(Figures S81–S83, Supporting Information).[21] As shown in Figure S80, Supporting Information, the hydrogen bond could be formed between the hydrogen atom of amino group of drug molecule and the oxygen atom of ester carbonyl group of *E* configuration fragment. Furthermore, the DFT calculation results showed that the interaction energy between drug molecule and *E* configuration fragment was –18.16 kcal mol^{-1}. The distance between the hydrogen atom of amino group and the oxygen atom of ester carbonyl group was 2.1 Å, indicating a strong hydrogen bond interaction between these two molecules. These results clearly indicate that JUC-556-$[HZ]_X$ (*E*) is a closed form for the drug adsorption. However, after being protonated, the ESP of oxygen atom of ester carbonyl group turned to be positive, which means the *Z* configuration fragment could not produce hydrogen bond with the drug (Figure S80, Supporting Information). According to the DFT calculation, the complex showed a strong electrostatic repulsive force, and thus the interaction energy between drug molecule and *Z* configuration fragment extremely dropped to 16.4 kcal mol^{-1}, which demonstrates that JUC-556-$[HZ]_X$ (*Z*) is an open form for drug release.

3. Conclusion

We have synthesized a series of novel 3D hydrazone-decorated COFs, JUC-556-$[HZ]_X$ (*E*), as pH-triggered rotary switches via the bottom–up multi-component approach. JUC-556-$[HZ]_X$ (*E*) showed high crystallinity, good chemical stability, and reversible *E*/*Z* isomerization at various pH values, verified by UV–vis absorption spectroscopy and proton conduction. Furthermore, these functionalized COF materials were applied to intelligent

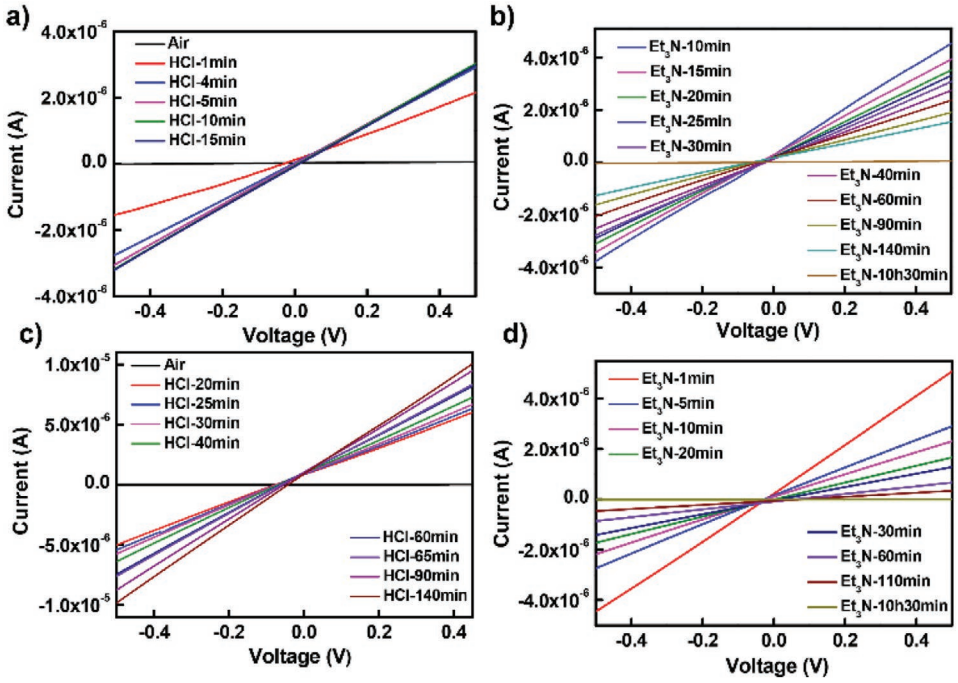

Figure 4. a) Proton conductivity of activated JUC-556-$[HZ]_{0.25}$ (*E*) in contact with HCl vapor. b) Proton conductivity of JUC-556-$[HZ]_{0.25}$ (*Z*) in contact with Et_3N vapor. c) Proton conductivity of activated JUC-556-$[HZ]_{0.50}$ (*E*) in contact with HCl vapor. d) Proton conductivity of JUC-556-$[HZ]_{0.50}$ (*Z*) in contact with Et_3N vapor.

pH-responsive Ara-C delivery and exhibited a nearly fourfold increase in the drug release at pH = 4.8 than at pH = 7.4, which will effectively improve drug-targeting and reduce drug side effects. This study thus develops the design and synthesis of 3D stimuli-responsive COFs, and promotes the potential application of COF materials for disease theragnostic.

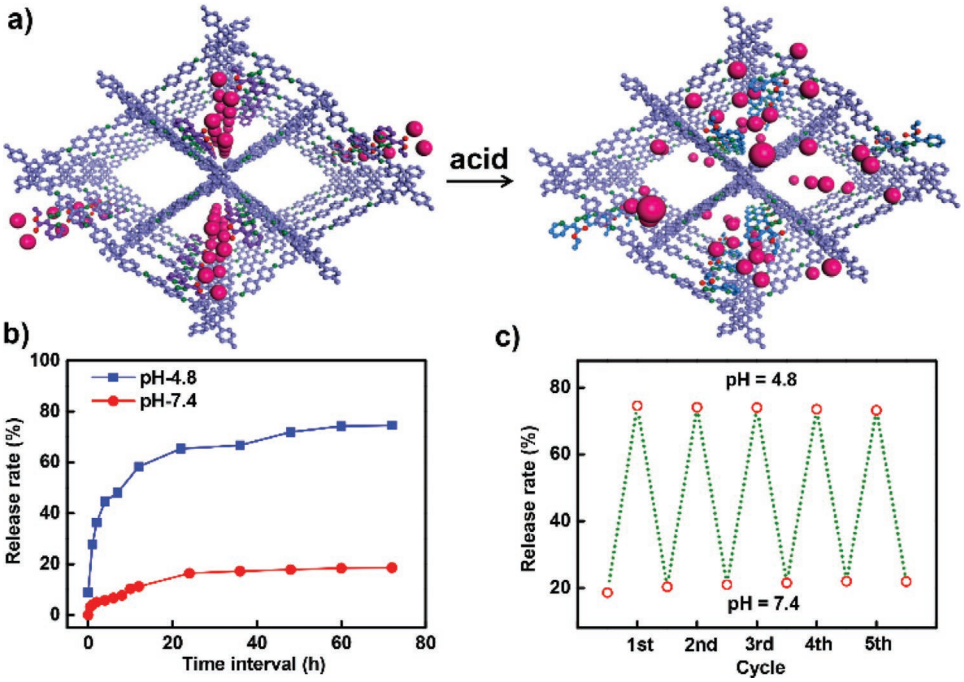

Figure 5. a) Schematic representation of the release of Ara-C from the channels of JUC-556-$[HZ]_X$ in acidic solution. b) Drug release profiles and c) reversibility of Ara-C-loaded JUC-556-$[HZ]_{0.50}$ in simulated cancer fluid (pH = 4.8 buffer solution) and in simulated normal body fluid (pH = 7.4 buffer solution).

4. Experimental Section

Synthesis of HZ (E): (*E*)-ethyl-2-(2-(4,4″-4,4″-dinitro-2-biphenylamine) hydrazono)-2-(pyridin-2-yl)acetate (HZ-NO_2, 1.5 g, 3.45 mmol, equivalent to NO_2 6.90 mmol), active carbon (0.225 g), hexahydrate ferric chloride (0.05 g, 0.185 mmol), and tetrahydrofuran (THF, 10.0 mL) were added into 100 mL three-necked round-bottomed flask with a magnetic stir-bar. Under a dried argon-flowing, the mixture was stirred rapidly and heated to 60 °C. Then, 80% hydrazine hydrate (0.875 mL, 14.35 mmol) was slowly added dropwise to the mixture and the resulting mixture was heated reflux for 8 h at 60 °C. The precipitation was washed in batches with 30.0 mL THF and added 40.0 mL ethyl acetate to the filtrate. The combined organic phases were washed four times with 40.0 mL saturated salt water, once with deionized water, and dried with $NaSO_4$. The solution was poured into 200.0 mL hexane, filtered, and removed solvent by rotary evaporation. The resulted red solid was purified by column chromatography (SiO_2: CH_2Cl_2/ ethyl acetate 8:1) to give HZ (0.90 g, 69%). ^{1}H NMR (400 MHz, DMSO): δ (ppm) 14.52 (s, 1 H), 8.06 (d, 1 H), 7.98 (d, 1 H), 7.89 (m, 1 H), 7.00 (d, 2 H), 6.96 (d, 1 H), 6.61 (d, 1 H), 6.69 (d, 2 H), 4.30 (q, 2 H), 1.35 (t, 3 H).

Synthesis of TFPA: 1,3,5,7-Tetraphenyladamantane (3.80 g, 8.6 mmol, 1 eq.) and dichloromethane (DCM, 150 mL) was added to a 250 mL three-necked round-bottomed flask with a magnetic stir-bar. Under a dried argon-flowing, the mixture was stirred rapidly and cooled to −10 °C with an ice/salt bath. Titanium tetrachloride (19.0 mL, 172.4 mmol, 20 eq.) was then added slowly to the mixture and stirred at −10 °C for 30 min. α, α-Dichloromethyl methyl ether (12.5 mL, 137.9 mmol, 16 eq.) was subsequently added dropwise to the mixture, which turned pale yellow during the addition. The reaction was held at −10 °C for 3 h and then allowed to warm to room temperature with stirring overnight. The mixture was poured into 300.0 mL ice-water, and 100.0 mL of 1 M HCl was added. Then, the resulting mixture was stirred for 30 min. During this time, the red/black organic phase turned bright yellow and some white precipitate was observed. The two-phase mixture was separated, and the aqueous phase was washed twice with 100.0 mL DCM. The combined organic phases were washed once with 100.0 mL of 1 M HCl, twice with deionized water, once with saturated aqueous $NaHCO_3$, once with saturated aqueous NaCl, and dried with $MgSO_4$. The solution was filtered and removed solvent by rotary evaporation. The resulted yellow solid was purified by column chromatography and then recrystallized from dioxane to give white to very pale-yellow crystals of TAPA. ^{1}H NMR (400 MHz, $CDCl_3$): δ (ppm) 10.02 (s, 1 H), 7.91 (d, 2 H), 7.67 (d, 2 H), 2.27 (s, 3 H).

Synthesis of JUC-556-[HZ]$_X$ (E): Dioxane/mesitylene (0.75 per 0.25 mL) mixtures of TFPA (0. 05 mmol, 28.1 mg) and HZ (*E*)/DABP (a total of 0.10 mmol) at different molar ratios of 0.25, 0.50, 0.75, and 1.00 in the presence of an acetic-acid catalyst (6 M, 0.1 mL) in a Pyrex tube (o.d. × i.d. = 10 × 8 mm^2) were flash frozen at 77 K (LN_2 bath), evacuated to an internal pressure of 0.15 mmHg and flame sealed. Upon sealing the length of the tube was reduced to ≈13 cm. The reaction mixture was heated at 120 °C for 3 days to afford an orange-yellow precipitate. The products were collected via filtration, washed six times with acetone (ACE, 20.0 mL). and then the activation solvent ACE was decanted and freshly replenished four times for 1 day to remove the trapped guest molecules. The powders were collected and dried at 120 °C under vacuum overnight to produce the corresponding JUC-556-[HZ]$_{0.25}$ (*E*), JUC-556-[HZ]$_{0.50}$ (*E*), JUC-556-[HZ]$_{0.75}$ (*E*), and JUC-556-[HZ]$_{1.00}$ (*E*) in the isolated yields of 80%, 79%, 81%, and 81%, respectively. Analytically calculated for JUC-556-[HZ]$_{0.25}$ (*E*): $C_{133}H_{101}N_{11}O_2$: C: 84.76; H: 5.36; N: 8.18. Found: C: 84.40; H: 5.13; N: 8.37. Analytically calculated for JUC-556-[HZ]$_{0.50}$ (*E*): $C_{142}H_{114}N_{14}O_4$: C: 82.00; H: 5.49; N: 9.43. Found: C: 82.41; H: 5.11; N: 9.42. Analytically calculated for JUC-556-[HZ]$_{0.75}$ (*E*): $C_{151}H_{127}N_{17}O_6$: C: 79.72; H: 5.59; N: 10.47. Found: C: 80.31; H: 5.01; N: 10.43. Analytically calculated for JUC-556-[HZ]$_{1.00}$ (*E*): $C_{160}H_{140}N_{20}O_8$: C: 77.80; H: 5.66; N: 11.35. Found: C: 78.54; H: 5.01; N: 11.28.

Supporting Information

Supporting Information is available from the Wiley Online Library or from the author.

Acknowledgements

This work was supported by the National Natural Science Foundation of China (22025504, 21621001, and 21390394), "111" project (BP0719036 and B17020), China Postdoctoral Science Foundation (2020TQ0118 and 2020M681034), and the program for JLU Science and Technology Innovative Research Team. V.V., Q.F., and S.Q. acknowledge the collaboration in the framework of China-French joint laboratory "Zeolites."

Conflict of Interest

The authors declare no conflict of interest.

Data Availability Statement

The data that support the findings of this study are available within the manuscript and the supporting information.

Keywords

covalent organic frameworks, drug release, functionalization, stimuli-responsive materials

Received: May 5, 2021
Revised: July 4, 2021
Published online:

[1] a) A. P. Cote, A. I. Benin, N. W. Ockwig, M. O'Keeffe, A. J. Matzger, O. M. Yaghi, *Science* **2005**, *310*, 1166; b) J. L. Segura, M. J. Mancheño, F. Zamora, *Chem. Soc. Rev.* **2016**, *45*, 5635; c) X.-Y. Guan, F.-Q. Chen, Q.-R. Fang, S.-L. Qiu, *Chem. Soc. Rev.* **2020**, *49*, 1357; d) K.-Y. Geng, T. He, R.-Y. Liu, S. Dalapati, K.-T. Tan, Z.-P. Li, S.-S. Tao, Y.-F. Gong, Q.-H. Jiang, D.-L. Jiang, *Chem. Rev.* **2020**, *120*, 8814.

[2] a) S.-S. Han, H. Furukawa, O. M. Yaghi, W. A. Goddard, *J. Am. Chem. Soc.* **2008**, *130*, 11580; b) H. Furukawa, O. M. Yaghi, *J. Am. Chem. Soc.* **2009**, *131*, 8875; c) S.-S. Yuan, X. Li, J.-Y. Zhu, G. Zhang, P. V. Puyveldeb, B. V. Bruggen, *Chem. Soc. Rev.* **2019**, *48*, 2665.

[3] a) X.-S. Ding, J. Guo, X. Feng, Y. Honsho, J.-D. Guo, S. Seki, P. Maitarad, A. Saeki, S. Nagase, D.-L. Jiang, *Angew. Chem., Int. Ed.* **2011**, *50*, 1289; b) M. Calik, F. Auras, L. M. Salonen, K. Bader, I. Grill, M. Handloser, D. D. Medina, M. Dogru, F. Löbermann, D. Trauner, A. Hartschuh, T. Bein, *J. Am. Chem. Soc.* **2014**, *136*, 17802; c) P.-P. Shao, J. Li, F. Chen, L. Ma, Q.-B. Li, M.-X. Zhang, J.-W. Zhou, A.-X. Yin, X. Feng, B. Wang, *Angew. Chem., Int. Ed.* **2018**, *57*, 16501.

[4] a) S.-Y. Ding, J. Gao, Q. Wang, Y. Zhang, W.-G. Song, C.-Y. Su, W. Wang, *J. Am. Chem. Soc.* **2011**, *133*, 19816; b) Q.-R. Fang, S. Gu, J. Zheng, Z.-B. Zhuang, S.-L. Qiu, Y.-S. Yan, *Angew. Chem., Int. Ed.* **2014**, *53*, 2878; c) H.-C. Ma, C.-C. Zhao, G.-J. Chen, Y.-B. Dong, *Nat. Commun.* **2019**, *10*, 3368.

[5] a) J.-P. Yu, L.-Y. Yuan, S. Wang, J.-H. Lan, L.-R. Zheng, C. Xu, J. Chen, L. Wang, Z.-W. Huang, W.-Q. Tao, Z.-Y. Liu, Z.-F. Chai, J. K. Gibson, W.-Q. Shi, *CCS Chem.* **2019**, *1*, 286; b) R.-R. Liang, F.-Z. Cui,

R.-H. A. , Q.-Y. Qi, X. Zhao, *CCS Chem.* **2020**, *2*, 139; c) Q.-R. Fang, Z.-B. Zhuang, S. Gu, R. B. Kaspar, J. Zheng, J.-H. Wang, S.-L. Qiu, Y.-S. Yan, *Nat. Commun.* **2014**, *5*, 4503; d) X.-Y. Guan, H. Li, Y.-C. Ma, M. Xue, Q.-R. Fang, Y.-S. Yan, V. Valtchev, S.-L. Qiu, *Nat. Chem.* **2019**, *11*, 587.

[6] a) H. M. El-Kaderi, J. R. Hunt, J. L. Mendoza-Cortés, A. P. Côté, R. E. Taylor, M. O'Keeffe, O. M. Yagh, *Science* **2007**, *316*, 268; b) Y.-B. Zhang, J. Su, H. Furukawa, Y.-F. Yun, F. Gándara, A. Duong, X.-D. Zou, O. M. Yaghi, *J. Am. Chem. Soc.* **2013**, *135*, 16336; c) Y.-Z. Liu, Y.-H. Ma, Y.-B. Zhao, X.-X. Sun, F. Gándara, H. Furukawa, Z. Liu, H.-Y. Zhu, C.-H. Zhu, K. Suenaga, P. Oleynikov, A. S. Alshammari, X. Zhang, O. Terasaki, O. M. Yaghi, *Science* **2016**, *351*, 365; d) T.-Q. Ma, E. A. Kapustin, S.-X. Yin, L. Liang, Z.-Y. Zhou, J. Niu, L.-H. Li, Y.-Y. Wang, J. Su, J. Li, X.-G. Wang, W.-D. Wang, W. Wang, J.-I. Sun, O. M. Yaghi, *Science* **2018**, *361*, 48.

[7] a) H. Li, J.-H. Chang, S.-S. Li, X.-Y. Guan, D.-H. Li, C.-Y. Li, L.-X. Tang, M. Xue, Y.-S. Yan, V. Valtchev, S.-L. Qiu, Q.-R. Fang, *J. Am. Chem. Soc.* **2019**, *141*, 13324; b) Q.-Y. Lu, Y.-C. Ma, H. Li, X.-Y. Guan, Y. Yusran, M. Xue, Q.-R. Fang, Y.-S. Yan, S.-L. Qiu, V. Valtchev, *Angew. Chem., Int. Ed.* **2018**, *57*, 6042; c) S.-C. Yan, X.-Y. Guan, H. Li, D.-H. Li, M. Xue, Y.-S. Yan, V. Valtchev, S.-L. Qiu, Q.-R. Fang, *J. Am. Chem. Soc.* **2019**, *141*, 2920; d) Z.-L. Li, H. Li, X.-Y. Guan, J.-J. Tang, Y. Yusran, Z. Li, M. Xue, Q.-R. Fang, Y.-S. Yan, V. Valtchev, S.-L. Qiu, *J. Am. Chem. Soc.* **2017**, *139*, 17771.

[8] C. Gao, J. Li, S. Yin, J.-L. Sun, C. Wang, *Nat. Commun.* **2020**, *11*, 4919.

[9] a) X. Su, I. Aprahamian, *Chem. Soc. Rev.* **2014**, *43*, 1963; b) S. M. Landge, E. Tkatchouk, D. Benítez, D. A. Lanfranchi, M. Elhabiri, W. A. Goddard, I. Aprahamian, *J. Am. Chem. Soc.* **2011**, *133*, 9812.

[10] a) S. Kassem, A. T. L. Lee, D. A. Leigh, A. Markevicius, J. Solà, *Nat. Chem.* **2016**, *8*, 138; b) S. M. Landge, I. Aprahamian, *J. Am. Chem. Soc.* **2009**, *131*, 18269; c) B.-H. Shao, M. Baroncini, H. Qian, L. Bussotti, M. D. Donato, A. Credi, I. Aprahamian, *J. Am. Chem. Soc.* **2018**, *140*, 12323; d) X. Su, S. Voskian, R. P. Hughes, I. Aprahamian, *Angew. Chem., Int. Ed.* **2013**, *52*, 10734.

[11] a) F. J. Uribe-Romo, C. J. Doonan, H. Furukawa, K. Oisaki, O. M. Yaghi, *J. Am. Chem. Soc.* **2011**, *133*, 11478; b) Z.-P. Li, N. Huang, K. H. Lee, Y. Feng, S.-S. Tao, Q.-H. Jiang, Y. Nagao, S. Irle, D.-L. Jiang, *J. Am. Chem. Soc.* **2018**, *140*, 12374; c) D. N. Bunck, W. R. Dichtel, *J. Am. Chem. Soc.* **2013**, *135*, 14952; d) L. Stegbauer, K. Schwinghammer, B. V. Lotsch, *Chem. Sci.* **2014**, *5*, 2789; e) X. Li, Q. Gao, J.-F. Wang, Y.-F. Chen, Z.-H. Chen, H.-S. Xu, W. Tang, K. Leng, G.-H. Ning, J.-S. Wu, Q.-H. Xu, S. Y. Quek, Y.-X. Lu, K. P. Loh, *Nat. Commun.* **2018**, *9*, 2335.

[12] C. Bonneau, O. Delgado-Friedrichs, M. O'Keeffea, O. M. Yaghi, *Acta Crystallogr. A* **2004**, *60*, 517.

[13] a) N. Huang, L.-P. Zhai, D. E. Coupry, M. A. Addicoat, K. Okushita, K. Nishimura, T. Heine, D.-L. Jiang, *Nat. Commun.* **2016**, *7*, 12325. b) N. Huang, X. Chen, R. Krishna, D.-L. Jiang, *Angew. Chem., Int. Ed.* **2015**, *54*, 2986.

[14] Materials Studio ver 7.0 Accelrys Inc., San Diego, CA.

[15] A. Nagai, Z.-Q. Guo, X. Feng, S.-B. Jin, X. Chen, X.-S. Ding, D.-L. Jiang, *Nat. Commun.* **2011**, *2*, 536.

[16] a) R. Kulkarni, Y. Noda, D. K. Barange, Y. S. Kochergin, P. Lyu, B. Balcarova, P. Nachtigall, M. J. Bojdys, *Nat. Commun.* **2019**, *10*, 3228; b) D. Chen, W.-B. Chen, G.-L. Xing, T. Zhang, L. Chen, *Chem. - Eur. J.* **2020**, *26*, 8377.

[17] a) N. Martinez, B. Drescher, H. Riehle, C. Cullmann, H. P. Vornlocher, A. Ganser, G. Heil, A. Nordheim, J. Krauter, O. Heidenreich, *BMC Cancer* **2004**, *4*, 44; b) M. S. Ghaji, Z. A. B. Zakaria, A. R. I. Shameha, M. H. M. Noor, H. Hazilawati, *J. Comput. Theor. Nanosci.* **2018**, *15*, 1128.

[18] a) J. H. Kim, Y. S. Kim, K. Park, S. Lee, H. Y. Nam, K. H. Min, H. G. Jo, J. H. Park, K. Choi, S. Y. Jeong, R. W. Park, I. S. Kim, K. Kim, I. C. Kwon, *J. Controlled Release* **2008**, *127*, 41; b) Y. Kato, S. Ozawa, C. Miyamoto, Y. Maehata, A. Suzuki, T. Maeda, Y. Baba, *Cancer Cell Int.* **2013**, *13*, 89.

[19] a) J. Chen, B. Zhang, F. Xia, Y.-C. Xie, S.-F. Jiang, R. Su, Y. Lua, W. Wu, *Nanoscale* **2016**, *8*, 7127; b) R. Ocampo-Pérez, M. Sánchez-Poloa, J. Rivera-Utrillaa, R. Leyva-Ramos, *Chem. Eng. J.* **2010**, *165*, 581; c) S. J. Sonawane, R. S. Kalhapure, T. Govender, *Eur. J. Pharm. Sci.* **2017**, *99*, 45.

[20] a) J. Zhang, *J. Chem. Theory Comput.* **2018**, *14*, 572; b) T. Lu, F. W. Chen, *J. Comput. Chem.* **2012**, *33*, 580.

[21] M. J. Frisch, G. W. Trucks, H. B. Schlegel, G. E. Scuseria, M. A. Robb, J. R. Cheeseman, G. Scalmani, V. Barone, B. Mennucci, G. A. Petersson, H. Nakatsuji, M. Caricato, X. Li, H. P. Hratchian, A. F. Izmaylov, J. Bloino, G. Zheng, J. L. Sonnenberg, M. Hada, M. Ehara, K. Toyota, R. Fukuda, J. Hasegawa, M. Ishida, T. Nakajima, Y. Honda, O. Kitao, H. Nakai, T. Vreven, J. A. Montgomery, J. E. Peralta, F. Ogliaro, M. Bearpark, J. J. Heyd, E. Brothers, K. N. Kudin, V. N. Staroverov, R. Kobayashi, J. Normand, K. Raghavachari, A. Rendell, J. C. Burant, S. S. Iyengar, J. Tomasi, M. Cossi, N. Rega, N. J. Millam, M. Klene, J. E. Knox, J. B. Cross, V. Bakken, C. Adamo, J. Jaramillo, R. Gomperts, R. E. Stratmann, O. Yazyev, A. J. Austin, R. Cammi, C. Pomelli, J. W. Ochterski, R. L. Martin, K. Morokuma, V. G. Zakrzewski, G. A. Voth, P. Salvador, J. J. Dannenberg, S. Dapprich, A. D. Daniels, Ö. Farkas, J. B. Foresman, J. V. Ortiz, J. Cioslowski, D. J. Fox, Gaussian 09, Rev. A.01, Gaussian, Inc., Wallingford, CT **2009**.